Advanced Encapsulants for Reduced Thermal Mechanical Stress in Photovoltaic Modules: A Quantitative Analysis Using FBGS

Peer-reviewed author version

VAN DYCK, Rik; CASASOLA PAESA, Marta; ENGELEN, Tine; LUO, Bin; BORGERS, Tom; GOVAERTS, Jonathan; SIVARAMAKRISHNAN RADHAKRISHNAN, Hariharsudan; DAENEN, Michael; POORTMANS, Jef & van Vuure, Aart Willem (2023) Advanced Encapsulants for Reduced Thermal Mechanical Stress in Photovoltaic Modules: A Quantitative Analysis Using FBGS. In: 2023 IEEE 50TH PHOTOVOLTAIC SPECIALISTS CONFERENCE, PVSC, IEEE, p. 1 -3.

DOI: 10.1109/PVSC48320.2023.10359569
Handle: http://hdl.handle.net/1942/42657

Advanced Encapsulants for Reduced Thermal Mechanical Stress in Photovoltaic Modules: A Quantitative Analysis Using FBGS

Rik Van Dyck[1,2,3,4], Marta Casasola Paesa[2,3,4], Tine Engelen[2,3,4] Bin Luo[1,2,3,4],Tom Borgers[2,3,4], Jonathan Govaerts[2,3,4], Hariharsudan Radhakrishnan[2,3,4], Michael Daenen[2,3,4], Jef Poortmans[1,2,3,4], Aart Willem van Vuure[1]

[1]KU Leuven, Leuven, Belgium, [2]Hasselt University, imo-imomec, Hasselt, Belgium, [3]imec, Genk, Belgium, [4]EnergyVille, Genk, Belgium

Abstract — In this work, two mini-modules using a 3D multi-ribbon interconnection are fabricated. One with TPO and the other with glass fiber reinforced TPO (GF TPO) encapsulant. Using fiber Braggs grating sensors (FBGS) attached to the cell, in situ temperature and strain are quantified during reliability tests in the form of thermal cycling from -40ºC to +85ºC. It was found that the temperature of the cell surface reaches -36ºC and +81ºC at its minimum and maximum respectively. The measured cell strain followed the same cycling behavior between tension and compression. The strain in the GF TPO based module was found to have a lower peak-to-peak (difference between max tension and compression) value. Also, a consistent difference between strain in parallel and perpendicular directions relative to the busbars was observed, with the latter one being larger.

I. INTRODUCTION

The effect of the coefficient of thermal expansion (CTE) mismatch between module materials on the thermal stress induction has mainly been studied using finite element simulations [1]–[3]. The actual quantification of these stresses is limited to using external measurements methods such as spectroscopy [4]. The use of a Fiber Braggs Grating Sensor (FBGS) as an in-situ strain and temperature quantification method for photovoltaic (PV) modules was recently proposed [4], [5]. It was shown that temperature and strain could be measured, without affecting the module's thermal mechanical behavior. Indeed, the small FBGS diameter (~100 µm) allows effective integration without changing the PV module buildup, hence there is no significant impact on the thermal mass or mechanical stability. Also, optically there is no significant effect on the photon transmission due to the limited diameter and matching refracting indices . A brief explanation of the working principle of the FBGS is outside the scope of this abstract.

This work uses module-integrated FBGS to quantify temperature and thermally induced strain during reliability tests in the form of thermal cycling. The tested modules use a 3D multi-ribbon interconnection for back-contact cells. The concept [6] and reliability assessments [7] of this technology were previously published. Both a mini module with thermoplastic polyolefin (TPO) and glass fiber reinforced TPO (GF TPO) encapsulant will be fabricated and tested. The research objective is to find the effect of the encapsulant reinforcement on the thermally induced strain within the module.

II. MATERIALS AND METHODS

Encapsulant material selection

Two encapsulants are studied and compared for this work, a commercially available TPO, and the same TPO, reinforced with 10 w% randomly oriented short glass fibers: the GF TPO. The fibers have a diameter ranging from 10 to 12 µm. While previous publications explained the benefit of the GF addition on its processability [6], this work focuses on the effect on the CTE, and its associated thermal induced stresses. A thermal mechanical analysis was performed on the encapsulants to determine their CTE as shown in Fig. 1. This shows the CTE-reducing effect of the glass fiber reinforcement, being larger at higher temperatures.

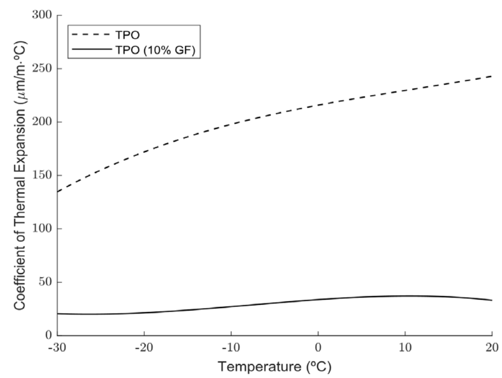

Fig. 1. Coefficient of thermal expansion (CTE) of a TPO and GF reinforced TPO as a function of temperature

Sample fabrication

For this work, two four-cell modules were studied. The architecture and fabrication procedure were identical, but one contains pure TPO encapsulant, while the other uses the GF TPO. Both modules were fabricated using a hand-made interconnection fabric of encapsulant with integrated metal ribbons. The metal ribbons have a copper core of 800x70 µm^2 and are coated in a 12 µm thick $Sn_{57}Bi_{42}Ag_1$ solder alloy, which has a melting temperature of 139 ºC. An exploded view of the layup phase is shown in Fig. 2.

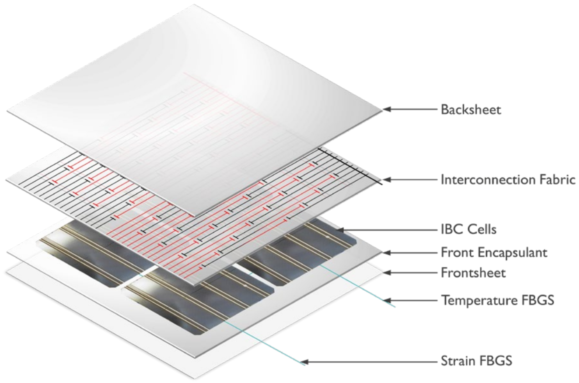

Fig. 2. Exploded view of the module layup

The established stack consists of a glass front sheet, encapsulant, four IBC cells, an interconnection fabric aligned to the cell metallization, and a glass backsheet. The front- and backsheet are both low Fe tempered 35x35 cm^2 glass plates with a thickness of 3 mm and without anti-reflection coating. During a lamination step, the stack is preheated to 165 °C in a vacuum for 10 minutes before 700 mbar of pressure is applied for 17 minutes using a membrane. An example picture of a module frontside is shown in Fig. 3(a).

Each module contains one strain and one temperature FBGS, which are attached to the front side of the cells using an adhesive before the lamination cycle. A schematic drawing of the configuration is shown in Fig. 3 (b), with the blue and red lines being the strain and temperature sensor respectively. The strain sensor has eight measuring points, two for each cell, allowing both X and Y direction strain quantification. The X direction corresponds to a measuring direction perpendicular to the busbars on the cell, while the Y direction corresponds to a measurement in parallel with the busbars

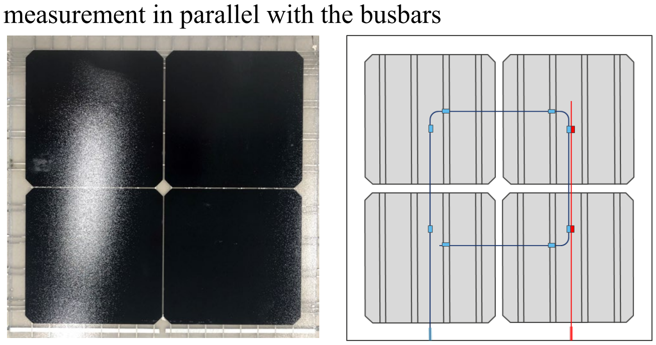

(a) (b)

Fig. 3. (a) picture of the frontside of a laminated four-cell module, (b) schematic drawing of the module, with the red and blue lines indicating the strain and temperature FBGS respectively.

FBGS calibration and used formulas

After lamination, the modules underwent a step cycle of heating and cooling in order to calibrate the temperature sensor. The step cycle consists of 7 heating and cooling steps, where during each step, the module was kept at a constant temperature for 4 hours. The set step cycle and resulting output wavelengths are shown in Fig. 4 (a). The average wavelength on each plateau was determined in order to find the wavelength-temperature combinations and fit the temperature as a function of the measured wavelength according to (1). The average wavelength and temperature data together with the fitted relationship are given in Fig. 4 (b).

$$T(\lambda) = T_{ref} - \frac{S_1}{2S_2} + \frac{S_2}{|S_2|} \cdot \sqrt{\left(\frac{S_1}{2S_2}\right)^2 + \frac{1}{S_2} \cdot \ln\left(\frac{\lambda}{\lambda_{ref}}\right)} \tag{1}$$

With T temperature, λ the measured wavelength, S_1 and S_2 the linear and quadric temperature sensitivity coefficients, T_{ref} and λ_{ref} the temperature and wavelength at a known reference point.

Based on this model and the calibration data, S_1 and S_2 were found to be 5.98×10^{-6} and 8.14×10^{-9} respectively, with an R^2 value of 0.99995. These values can be filled in (2) in order to obtain a relationship between measured wavelength and strain.

$$\varepsilon(\lambda) = \frac{1}{k}\left[\ln\left(\frac{\lambda}{\lambda_0}\right) - S_1(\Delta T_0) - S_2(\Delta T_0)^2\right] - (\alpha_{si} - \alpha_f)(\Delta T_0) \tag{2}$$

With

$$\Delta T_0 = T - T_0$$

and ε the actual strain, k the gage factor (7.77×10^{-7}), α_{si} and α_f the CTE of the Si cell (3.5×10^{-6} /ºC) and FBGS (0.5×10^{-6} /ºC) respectively.

This equation will be used in order to calculate the measured strain during thermal cycling according to the IEC 61215.2021 standard [8]. A total of 175 thermal cycles have been performed and monitored. Also, the temperature profile during the lamination cycle, showing the different stages has been measured.

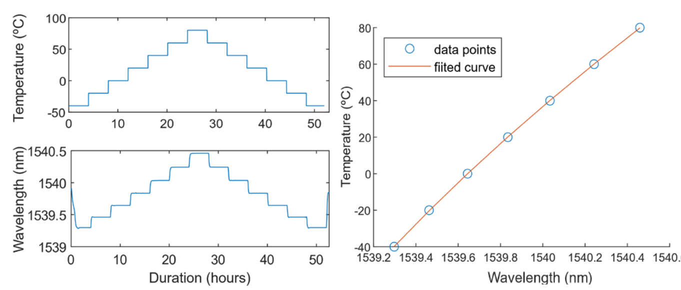

(a) (b)

Fig. 4. (a) Set temperature profile during the calibration cycle (top) and measured wavelengths of the temperature sensor (bottom), (b) fitted temperature-wavelength relationship according to (1)

III. Results and Discussion

Fig. 5. shows the measured (in module) and climate chamber (ambient) temperature and strain for one cell of both module during one thermal cycle. This is a zoom-in on one cycle during the first 24-hour thermal cycling test of 8 cycles. Similar results were observed for the 7 other cycles during this test. Both the in-module temperature and strain are calculated from the output wavelength using the equations discussed above, the strain being referenced to the module at 25 ºC. The minimum and

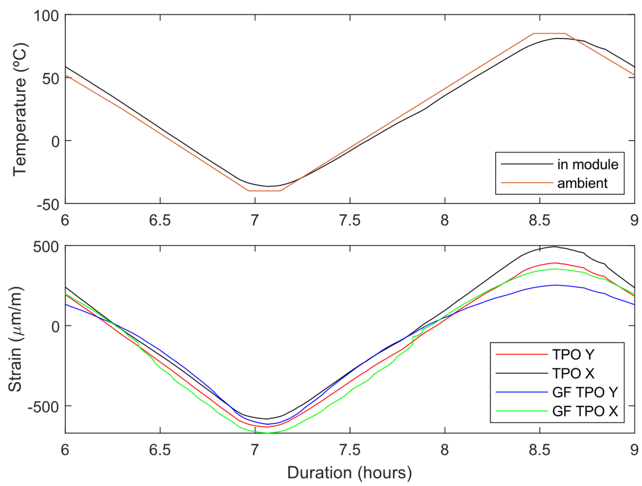

Fig. 5. Measured and set temperature (top) and strain (bottom) for one cell in X and Y direction during one thermal cycle, both for a module with TPO and GF TPO encapsulant

maximum in module temperatures are -36ºC and 81ºC degrees respectively, resulting in an offset with the set temperature profile of 4ºC at these maxima.

When cooling down the module, the strain values go negative, which corresponds to compression. This is expected due to the larger CTE of the encapsulant compared to the Si cell. The encapsulant is attached to the cell, so during cooling, it pulls the cells into compression. The opposite happens during the heating cycle of the module. As mentioned above, the Y and X direction corresponds to the parallel and perpendicular directions compared to the busbars on the cell respectively.

TABLE 1 gives the maximum strain values in tension and compression. The peak-to-peak difference, in other words, the total strain variation to which the cell is exposed, is significantly smaller for the module with GF TPO encapsulant. The difference between the TPO and GF TPO module in compression is rather limited, with 36 and 31 µm/m for the X and Y direction respectively. A larger difference is observed in tension mode, with the difference being 140 and 139 for X and Y direction respectively. This might be attributed to the smaller CTE difference for the TPO and GF TPO at low temperatures compared to higher temperatures, as shown above in Fig. 1.

TABLE 1
MAXIMUM STRAIN DURING ONE THERMAL CYCLE IN COMPRESSION AND TENSION

	Compression (µm/m)	**Tension (µm/m)**	**Difference (µm/m)**
TPO X	631	492	1123
TPO Y	580	391	971
GF TPO X	668	352	1020
GF TPO Y	611	252	863

Overall, the observed strain in compression is higher than in tension. This could again be attributed to the behavior of the encapsulant material behaving like a solid at lower temperatures and becoming more viscous at higher temperatures. This more viscous behavior can result in more internal slip in the polymer, resulting in stress relief. Dynamic mechanical analysis to show the viscous behavior is performed and results could be included in the final paper.

Longer thermal cycling tests (up to 100 cycles) are performed, and strain measurement results will be included in the final paper. Changes in strain during these tests can be an indication of degradation of the module. Also electrical characterization of the modules can be included.

IV. CONCLUSIONS

This work was able to utilize a previously proposed approach to incorporate FBGS in a PV mini-module in order to quantify temperature and strain during thermal cycling. Adding glass fiber reinforcement to a TPO encapsulant has been shown to reduce the strain on cell level, both in parallel and perpendicular directions to the busbars. This can be attributed to the reduction in CTE due to the glass fiber reinforcement, reducing the CTE mismatch in the module.

V. REFERENCES

[1] L. Yixian and A. A. O. Tay, "Finite element thermal stress analysis of a solar photovoltaic module," in *2011 37th IEEE Photovoltaic Specialists Conference*, 2011, pp. 3179–3184. doi: 10.1109/PVSC.2011.6186616.

[2] O. O. Ogbomo *et al.*, "Effect of Coefficient of Thermal Expansion (CTE) Mismatch of Solder Joint Materials in Photovoltaic (PV) Modules Operating in Elevated Temperature Climate on the Joint's Damage," *Procedia Manuf*, vol. 11, pp. 1145–1152, 2017, doi: 10.1016/j.promfg.2017.07.236.

[3] U. Eitner *et al.*, "Thermal Stress and Strain of Solar Cells in Photovoltaic Modules," in *Shell-like Structures: Non-classical Theories and Applications*, Ed: Springer Berlin Heidelberg, 2011, pp. 453–468.

[4] P. Nivelle *et al.*, "The Lamination Process Quantified Through In-Situ Optical Thermo-Mechanical Sensing," in *Proceedings in the WCPEC 8*, 2022.

[5] P. Nivelle *et al.*, "In situ quantification of temperature and strain within photovoltaic modules through optical sensing," *Prog. Photovolt.: Res. Appl.*, pp. 1–7, 2022, doi: 10.1002/pip.3622.

[6] R. van Dyck *et al.*, "Three-dimensional multi-ribbon interconnection for back-contact solar cells," *Prog. Photovolt.: Res. Appl.* vol. 29, no. 5, pp. 507–515, 2021, doi: https://doi.org/10.1002/pip.3390.

[7] R. van Dyck *et al.*, "Three-Dimensional Multi-Ribbon Back-Contact Interconnection: Latest Results on Reliability Testing," in *38th EUPVSEC*, 2021, pp. 728–731.

[8] "IEC 61215-1 Terrestrial photovoltaic modules – Design qualification and type approval," 2021.